The Role of Tyr41 and His155 in the Functional Properties of Superoxide Dismutase from the Archaeon *Sulfolobus solfataricus*†

Maria Angela Gogliettino,‡ Fabio Tanfani,§ Ancrea Sciré,§ Thomas Ursby,|| Bianca Stella Adinolfi,‡ Tiziana Cacciamani,§ and Emmanuele De Vendittis*,‡

Dipartimento di Biochimica e Biotecnologie Mediche, Università di Napoli Federico II, Via S. Pansini, 5, I-80131 Napoli, Italy, Istituto di Biochimica, Facoltà di Scienze, Università Politecnica delle Marche, Via Ranieri, I-60131 Ancona, Italy, and MAX-Lab, Lund University, P.O. Box 118, S-22100 Lund, Sweden

Received September 15, 2003; Revised Manuscript Received December 22, 2003

ABSTRACT: We have examined and compared the effects of mutating Y41 and H155 in the iron superoxide dismutase (SOD) from the archaeon *Sulfolobus solfataricus* (*Ss*). These two neighboring residues in the active site are known to have crucial functions in structurally related SODs from different sources. The metal analysis indicates a slightly lower iron content after either Y41F or H155Q replacement, without any significant substitution of iron for manganese. The specific activity of *Ss*SOD referred to the iron content is 17-fold reduced in the Y41F mutant, whereas it is less than 2-fold reduced by the H155Q mutation. The noticeable pH dependence of the activity of *Ss*SOD and H155Q-*Ss*SOD, due to the ionization of Y41 (p*K* 8.4), is lost in Y41F-*Ss*SOD. After H155Q and even more after the Y41F substitution, the archaeal enzyme acquires a moderate sensitivity to sodium azide inhibition. The hydrogen peroxide inactivation of *Ss*SOD is significantly increased after H155Q replacement; however, both mutants are insensitive to the modification of residue 41 by phenylmethanesulfonyl fluoride. Heat inactivation studies showed that the high stability of *Ss*SOD is reduced by the H155Q mutation; hovewer, upon the addition of SDS, a much faster inactivation kinetics is observed both with wild-type and mutant *Ss*SOD forms. The detergent is also required to follow thermal denaturation of the archaeal enzyme by Fourier transform infrared spectroscopy; these studies gave information about the effect of mutations and modification on flexibility and compactness of the protein structure. The crystal structure of Y41F mutant revealed an uninterrupted hydrogen bond network including three solvent molecules connecting the iron-ligating hydroxide ion via H155 with F41 and H37, which is not present in structures of the corresponding mutant SODs from other sources. These data suggest that Y41 and H155 are important for the structural and functional properties of *Ss*SOD; in particular, Y41 seems to be a powerful regulator of the activity of *Ss*SOD, whereas H155 is apparently involved in the organization of the active site of the enzyme.

Studies on SODs[1] isolated from several sources point to the key role played by this metal enzyme in the protection against the toxicity of superoxide anions produced during oxidative stress (*1*−*3*). Its properties and classification in structurally unrelated families have been extensively reviewed (*3*−*8*). *Ss*SOD isolated from the hyperthermophilic archaeon *Sulfolobus solfataricus* is an iron-containing enzyme endowed with a high heat resistance (*9*). *Ss*SOD is insensitive to sodium azide inhibition (*9*, *10*), but it is inactivated by hydrogen peroxide treatment (*9*). Its 3D-structure showed that the enzyme is organized as a very compact homotetramer with an overall fold of the monomer similar to that of structurally related SODs containing either Fe or Mn in the active site (*11*). The crystal structure of *Ss*SOD also revealed the presence of a covalent modification of Y41 (*11*), a conserved residue of Fe- and Mn-SODs located in the channel that drives the superoxide anion to the active site (*12*). In *Ss*SOD the modification is caused by phenylmethanesulfonyl fluoride (PMSF), that reacts with the hydroxy group of Y41 and causes the irreversible inactivation of the enzyme (*13*). A similar reactivity was previously reported for the corresponding Y34 of human mitochondrial Mn-SOD (*14*). However, in this case the modifying agent was peroxynitrite, which led to the formation of a 3-nitrotyrosine (*14*−*16*). This highly reactive tyrosine residue plays an important role in the mechanism of superoxide dismutation through deprotonation of its hydroxy group, as confirmed by mutagenic studies on Fe-SOD from *Escherichia coli* (*17*, *18*) and human mitochondrial Mn-SOD (*19*). A recent study on Fe- and Mn-SOD from *E. coli* showed that these enzymes have a very similar proton-coupled electron transfer upon reduction of the SOD active site, the proton acceptor of the oxidized enzyme (Fe^{3+}−SOD or Mn^{3+}−SOD) being the ionized solvent molecule coordinating the metal ion (*20*).

† The work was supported by Ministero dell'Università e della Ricerca Scientifica e Tecnologica (Rome), PRIN 2003.

* To whom correspondence should be addressed: Telephone: +39.081.7463118. Fax: +39.081.7463653. E-mail: devendittis@dbbm.unina.it.

‡ Università di Napoli Federico II.

§ Università Politecnica delle Marche.

|| Lund University.

[1] Abbreviations: SOD, superoxide dismutase; *Ss*, *Sulfolobus solfataricus*; PMSF, phenylmethanesulfonyl fluoride; FT-IR, Fourier transform infrared; Amide I′, Amide I band in ^2H_2O medium.

10.1021/bi035661y CCC: $27.50
Published on Web 02/06/2004

Another crucial position for the structure of the active site of Fe- and Mn-SODs is occupied by H155 in *Ss*SOD (*11*). H155 is close to Y41 and to the metal binding coordination sphere of the enzyme (*11*, *12*, *21*, *22*). While Y41 is strictly conserved, the position of H155 is occupied by a histidine or glutamine, the glutamine being in the sequence position corresponding to either G80 or H155 (in *Ss* numbering). This residue hydrogen bonds to the hydroxy group of the conserved tyrosine residue. Also in the crystal structure of the PMSF-modified *Ss*SOD, H155 forms a hydrogen bond with Y41 (*11*, *13*). The hypothesis that His/Gln in the position of H155 (both in sequence and structure) implies a SOD active with Fe/Mn, respectively, was weakened by the occurrence of SODs with a histidine residue in this position, capable of functioning with either Fe or Mn (*23*). Furthermore, the H145Q mutant in Fe-SOD from *Mycobacterium tuberculosis* led to a mutant retaining the iron atom (*24*). Surprisingly, in the H145E mutant the manganese replaced the iron atom, thus suggesting that this alteration in metal specificity reflects the preference of manganese ions for anionic ligands (*24*). Probably, also oher residues are involved in the metal specificity, as demonstrated for the cambialistic SOD from *Porphyromonas gingivalis*. In this case, a glycine apart from the active site (G155 in *P. gingivalis* SOD), conserved in most Mn-SODs, was replaced by a threonine residue, mostly found in Fe-SODs; that substitution changed the metal specificity of the enzyme from a cambialistic type to one close to an iron-specific type (*25)*.

In this work the availability of a suitable expression system for the production of recombinant *Ss*SOD (*13*) prompted us to carry out the mutagenic analysis of Y41 and H155. The investigation of the role of these residues in the archaeal enzyme could allow a deeper insight into the regulation of the properties of the Fe- and Mn-SOD family, through the evaluation of the effects of analogous mutations in different organisms. Under this aspect, the archaeon *Ss* represents a suitable model for studying the evolution of this ancient and crucial scavenger of toxic radicals developed for the protection against the toxicity related to oxygen consumption. The comparison between *Ss*SOD and the mammalian mitochondrial Mn-SOD could be particularly interesting. In fact, the mammalian enzyme shares with *Ss*SOD (i) a compact homotetrameric organization (*11*, *22*), (ii) a 38% amino acid sequence identity (*11*), (iii) a similar reactivity toward covalent modifications (*13*, *14*), and (iv) an unusual heat resistance for a mesophilic enzyme (*26*). Furthermore, the *Sulfolobus* genus has been proposed as the putative ancestor of animal mitochondria (*27*).

The amino acid substitutions carried out on *Ss*SOD were Y41F and H155Q, and the corresponding mutated forms were purified and characterized in comparison with wild-type *Ss*SOD or its PMSF-modified form. The data obtained indicate that the free hydroxy group of Y41 has a more crucial role in the catalytic mechanism of superoxide dismutation, as compared to mammalian or bacterial sources, and that H155 is involved in keeping a correct structural organization of the active site of *Ss*SOD, together with the fact that this residue modifies the reactivity of Y41.

MATERIALS AND METHODS

Chemicals, Enzymes, and Buffers. Chromatographic media and columns were from Pharmacia Biotech or Biorad. Restriction/modifying enzymes were from Amersham or Promega. Oligonucleotides were synthesized by Genset (Paris, France). Xanthine, xanthine oxidase, cytochrome *c*, and PMSF were purchased from Sigma-Aldrich. Deuterium oxide (99.9 % ^2H_2O), ^2HCl, and NaO^2H were from Aldrich. The stock solution of PMSF was prepared in ethanol to avoid its inactivation in aqueous solution. All other chemicals were of analytical grade.

Methods. Transformation of bacterial strains, preparation of plasmids through the use of the Qiagen kits (M-Medical), and other details of DNA recombinant technology were as described (*28*). PCR amplifications of DNA segments were carried out on DNA Thermal Cycler from Perkin-Elmer. Nucleotide sequencing was performed using the T7 sequencing kit from Pharmacia Biotech.

Samples of recombinant or mutated *Ss*SOD were stored in 20 mM Tris·HCl buffer pH 7.5, containing 50% (v/v) glycerol. SOD activity was measured at 25 °C by the inhibition of the cytochrome *c* reduction caused by superoxide anions generated with the xanthine/xanthine oxidase method (*9*, *29*). One unit of SOD activity was defined as the amount of enzyme that caused 50% inhibition of cytochrome *c* reduction. Unless otherwise indicated, the standard buffer used for the reaction was 100 mM potassium phosphate, pH 7.8, containing 0.1 mM Na_2EDTA. When different buffers were used to measure SOD activity, the xanthine/xanthine oxidase method was adjusted to give a rate of cytochrome *c* reduction similar to that measured at pH 7.8. The pH interval covered by the different buffers was 5.5−10.85 with some overlapping points. Protein concentration was determined by the method of Bradford (*30*), using bovine serum albumin as standard. Protein purity was evaluated by SDS/PAGE (*31*). The tetrameric structure of the mutant forms of *Ss*SOD was evaluated by gel filtration on a Superdex 75 HR 10/30 column calibrated with *Ss* proteins as molecular-size markers (*11*).

The metal content in protein solutions was determined by flame atomic absorption spectrometry, using a Varian SpectrAA 220 atomic absorption spectrometer equipped with a MK7 burner. Solutions were directly aspired into an air-acetylene flame with no prior treatment or after dilution in 20 mM Tris·HCl buffer pH 7.5. Concentrations were obtained by comparison with calibration curve and also by standard addition.

Preparation of Recombinant SsSOD and Its Mutant Forms Containing Y41F or H155Q Amino Acid Replacement. Recombinant *Ss*SOD was obtained through the expression system previously described (*13*), constituted by the host *Escherichia coli* strain JM109(DE3) (Novagen) transformed with the vector vSOD engineered from the plasmid pT7-7 (USB).

The production of the mutant forms of *Ss*SOD was obtained through the site-directed mutagenesis on the corresponding gene cloned in the vector vSOD. The first target triplet, $T_{124}AT$ (coordinates of the *Ss*SOD gene including the start codon, see ref *13*), was mutagenised into $T_{124}TT$, to obtain the Y41F amino acid replacement (amino acid numbering excludes initial methionine missing in native *Ss*SOD, see ref *9*). Using vSOD as template, a 232 bp segment was amplified with the direct primer 5′d-A_{-97}TTCGAACTTCTGATAGACT$_{-78}$-3′ and reverse primer 5′d-T_{135}CCATTTACAAAGCCTTTATG$_{115}$-3′, whereas

another 571 bp segment was obtained with the primers 5′-C_{115}ATAAAGGCTTTGTAAATGGA$_{135}$-3′ and 5′-A_{685}-ATTGCGGATACCATACTAA$_{666}$-3′ (the designed mismatch is underlined). The amplified segments were purified on 1% agarose gel and then mixed at equimolar amounts; after melting of the fragments, reannealing was achieved in the overlapping 21-mer region containing the mutated triplet. The heteroduplex with recessed 3′-ends was extended by *Taq* DNA polymerase and amplified using the direct primer 5′d-A_{-97}TTCGAACTTCTGATAGACT$_{-78}$-3′ and the reverse primer 5′-A_{685}ATTGCGGATACCATACTAA$_{666}$-3′. The resulting 782 bp segment was shortened to 524 bp via double digestion with *Nde*I and *Sph*I and cloned in the 2.7 kbp *Sph*I→*Nde*I fragment prepared from vSOD. The new plasmid was called vSOD(Y41F). The target triplet for the H155Q amino acid replacement is C_{466}AC, and its conversion into C_{466}AG was obtained by using the Quick Change mutagenesis kit from Stratagene. The method entailed the amplification of the entire vSOD vector with the DNA polymerase PfuTurbo, using primers annealing in the target region, namely, 5′d-T_{457}TCGAAAATCAGTTCCAAAATC$_{478}$-3′ and 5′d-G_{478}ATTTTGGAACTGATTTTCGAA$_{457}$-3′. The amplification product was digested with the restriction endonuclease *Dpn*I to remove non mutated DNA plasmid and then used to transform the super competent Epicurian Coli XL1-Blue cells. The new plasmid was called vSOD(H155Q). The structure of the mutant plasmids was identical to that of vSOD and contained the designed mutated triplet, as confirmed by nucleotide sequencing of the synthetic region. The expression of the new plasmids and the purification of recombinant mutated forms of *Ss*SOD was carried out as previously described for recombinant *Ss*SOD (*13*). The yield of purified mutant enzymes was similar to that reported for wild type *Ss*SOD (*13*).

Infrared Spectroscopy. The structure of proteins was analyzed in 50 mM Tris·HCl buffer pH or p^{2}H 7.8, in the absence or in the presence of 5.6% SDS (w/v). The p^{2}H corresponds to the pH meter reading +0.4 (*32*). Concentrated protein samples for infrared analysis were prepared as described (*33*) using centricon-30 micro concentrators (Amicon). Approximately 35 μL of the concentrated protein solution (3−3.5% w/v) was placed between two CaF_2 windows separated by 6 or 25 μm spacers for measurements in ^1H_2O or ^2H_2O medium, respectively. The windows were fitted in a thermostated Graseby Specac 20500 cell (Graseby-Specac Ltd, Orpington, Kent, UK). Fourier transform infrared (FT-IR) spectra were recorded by means of a Perkin-Elmer 1760-x FT-IR spectrometer using a deuterated triglycine sulfate detector and a normal Beer-Norton apodization function (*33*). Spectra were processed using the "Spectrum" software from Perkin-Elmer. The deconvoluted parameters for the Amide I band were set with a gamma value of 2.5 and a smoothing length of 60.

Crystallography. Crystals of Y41F-*Ss*SOD were grown under similar conditions to the PMSF-modified *Ss*SOD crystals (*11*). Crystals were grown by vapor diffusion in hanging drops at 21°C in a 1:1 mix of the reservoir solution (8% PEG 8000, 0.1 M Tris/HCl pH 8.5) and a protein solution (1.45 mg/mL Y41F-*Ss*SOD, 20 mM Tris/HCl pH 7.8, 1% glycerol). Data were collected at 100 K at beamline I711 (*34*) with $\lambda = 0.986$ Å using a Mar 345 image plate detector. Data were processed with XDS (*35*). The PMSF-modified *Ss*SOD model (PDB entry 1SSS) without solvent molecules and with residue 41 modeled as alanine was used as starting model. The structure was refined using Refmac (*36*) and CNS (*37*). Manual model rebuilding was done with O (*38*). Data collection and refinement statistics are shown in Tables 1 and 2.

Table 1: Data Collection Statistics for the Y41F-*Ss*SOD Mutant

space group	C2
unit cell parameters	
a (Å)	75.2
b (Å)	121.8
c (Å)	59.4
β (deg)	128.7
resolution limits (Å)	60.9−2.24
R_{sym}[a] (last shell 2.39−2.24 Å)	9.3% (25.5%)
$\langle I/\sigma \rangle$ (last shell 2.39−2.24 Å)	13.6 (5.2)
redundancy	4.1
number of unique reflections	19,994
fraction unique reflections with $I > 3\sigma(I)$	83%
completeness	99.7%

[a] $R_{sym} = \sum_h \sum_i |I_{h,i} - I_h| / \sum_h \sum_i I_{h,i}$.

Table 2: Refinement and Model Statistics for the Y41F-*Ss*SOD Mutant

no. of monomers per asymmetric unit	2
solvent content	47%
no. of unique reflections (excluding the test set)	19 994 (18 971)
no. of non-hydrogen atoms per dimer	3344
no. of solvent molecules in asymmetric unit with/without NCS mate	96/111
no. of non-hydrogen atoms in asymmetric unit	3551
crystallographic *R*-factor (R_{free})	0.180 (0.222)
rms deviation from ideal bond lengths (Å)	0.006
ideal angles/dihedrals/impropers	1.33/21.7/0.754
Ramachandran plot, residues	
in most favored regions	90.7%
in disallowed regions	0%
average B_{iso} main chain (1640 atoms)	16.4 Å^2
side chain (1702 atoms)	16.8 Å^2
iron (2 atoms)	17.9 Å^2
solvent (207 atoms)	32.9 Å^2

RESULTS

Molecular and Functional Properties of SsSOD after Y41F or H155Q Amino Acid Replacements. Y41F-*Ss*SOD and H155Q-*Ss*SOD showed the same electrophoretic mobility of recombinant *Ss*SOD, corresponding to a molecular mass of 24 kDa of the monomer subunit. The M_r was also determined under native conditions by gel-filtration chromatography, using a column calibrated with purified *Ss* proteins with known molecular size (*11*). Both mutant enzymes eluted as a single peak with an apparent M_r 87 900, a value approaching the theoretical value of a homotetramer. Therefore, the structural organization of *Ss*SOD in four identical subunits is maintained after Y41F or H155Q amino acid replacement.

The activity of Y41F-*Ss*SOD and H155Q-*Ss*SOD was first measured in standard buffer. The Y41F replacement causes a significant drop of the specific activity of *Ss*SOD, thus approaching the minimum activity levels determined on samples almost completely modified by the PMSF treatment (*13*). On the other hand, a good level of activity is maintained after the H155Q replacement, as it causes only a half-reduction of the specific activity. Further insight into the catalytic properties of the mutant *Ss*SOD forms was obtained through the study of the pH dependence of the activity

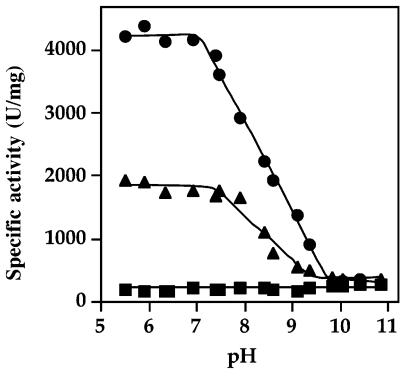

FIGURE 1: pH dependence of the specific activity of wild type *Ss*SOD and its mutant forms. Purified samples of *Ss*SOD (●), Y41F-*Ss*SOD (■), and H155Q-*Ss*SOD (▲) were assayed for SOD activity as indicated in Materials and Methods, with the exception that the standard buffer was replaced by the following buffered solutions, containing 0.1 mM Na_2EDTA: 50 mM MES·KOH, pH 5.5, 5.9, or 6.35; 50 mM imidazolium·HCl, pH 6.4, 6.9, or 7.45; 50 mM Tris·HCl, pH 7.4, 7.9, or 8.4; 50 mM glycine·HCl, pH 8.6, 9.1, 9.35, or 9.85; CAPS·KOH, pH 10.05, 10.4, or 10.85. The specific activity was expressed as U/mg protein.

(Figure 1). The profile obtained with *Ss*SOD is typical of an acid−base titration of a single acidic group, because above pH 7.4, the high level of specific activity of *Ss*SOD drops in the pH interval 7.4−9.4 and reaches a constant low value above pH 9.4. On the basis of similar results obtained on the Y34 residue of Fe-SOD from *E. coli* (*17*), we conclude that the acid candidate is the hydroxy group of Y41 and that its ionization has an apparent p*K* of 8.4. This conclusion is strengthened by the insensitivity of Y41F-*Ss*SOD to pH regulation, because the low activity of this mutant remains unchanged in the whole 5.5−10.85 pH interval (Figure 1). Furthermore, the pH dependence of a partially PMSF-modified *Ss*SOD sample is similar to that of unmodified *Ss*SOD, even though a lower activity was determined in the 5.5−7.4 pH interval (not shown). The pH dependence profile of H155Q-*Ss*SOD (Figure 1) is similar to that of *Ss*SOD, with the exception of the lower activity levels determined in the 5.5−7.4 pH range. This behavior suggests that the H155Q replacement has no influence on the deprotonation mechanism of Y41, whose p*K* remains unchanged. It is interesting that wild-type, modified, and mutant enzymes have a very similar low-activity values above pH 9.4. All these findings on the pH dependence of the different *Ss*SOD forms are based on the observation made by the indirect method used to measure SOD activity.

It has been reported that *Ss*SOD isolated from *S. solfataricus* cell extracts is an iron-containing enzyme on the basis of its metal content of 0.7 atoms of iron per subunit, the missing metal for the 1:1 stoichiometry being zinc (*9*). Table 3 reports the metal content of recombinant wild-type and mutant *Ss*SOD forms. In the wild-type enzyme, the amount of 0.63 iron atoms per subunit is similar to the value found in the endogenous enzyme. On the other hand, a moderately lower iron content is present after Y41F or H155Q replacement (0.47 or 0.46 atoms per subunit, respectively). The analysis on the metal content was extended to manganese to exclude an alteration of the metal selectivity caused by the mutations. However, as reported in Table 3, wild-type and mutant *Ss*SOD forms display a very similar low manganese content, ranging from 0.07 to 0.09 atoms per

Table 3: Activity and Metal Content of Wild-Type and Mutant Forms of *Ss*SOD

		metal content[a]	
sample	specific activity[b]	Fe	Mn
wild-type	6720 ± 140	0.63 ± 0.01	0.07 ± 0.01
Y41F mutant	387 ± 32	0.47 ± 0.01	0.08 ± 0.01
H155Q mutant	3980 ± 170	0.46 ± 0.01	0.09 ± 0.01

[a] Mean values ± SD are expressed as mol of Fe or Mn·mol subunit^{-1}. [b] The specific activity is expressed as U·mg protein^{-1}·mol of Fe^{-1}·mol subunit. Figures were calculated from the mean activity values ± SD obtained in the 5.5−7.4 pH interval (Figure 1).

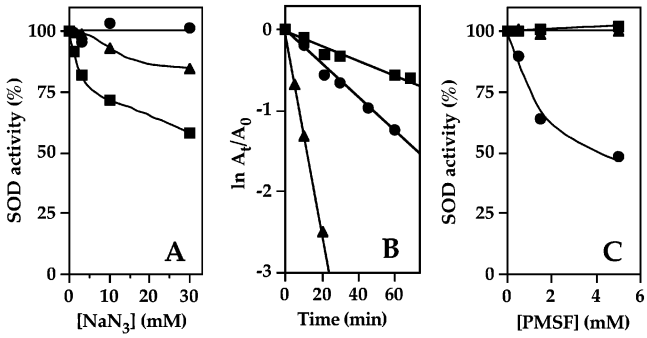

FIGURE 2: Effect of inhibitors and inactivators on the activity of wild type and mutant forms of *Ss*SOD. (A) The activity of *Ss*SOD (●), Y41F-*Ss*SOD (■), and H155Q-*Ss*SOD (▲) was mesaured in standard buffer in the presence of the indicated sodium azide concentrations. For each *Ss*SOD form the activity was expressed as a percentage of the activity measured in the absence of sodium azide. (B) Solutions of 0.1 mg/mL *Ss*SOD (●), Y41F-*Ss*SOD (■), and H155Q-*Ss*SOD (▲) in standard buffer were incubated at 25 °C in the presence of 0.5 mM H_2O_2. At the times indicated, aliquots were withdrawn from the reaction mixtures and assayed for residual SOD activity as described in Materials and Methods. The data were plotted according to the equation of a first-order kinetics, where A_0 or A_t represents the activity measured at the time zero or *t*, respectively. (C) Solutions of 0.1 mg/mL *Ss*SOD (●), Y41F-*Ss*SOD (■), and H155Q-*Ss*SOD (▲) in standard buffer were incubated at 25 °C for 30 min in the presence of the indicated concentrations of PMSF. Aliquots of the treated samples were assayed for residual SOD activity as described in Materials and Methods. The activity was expressed as a percentage of the activity measured in the absence of PMSF.

subunit. This finding indicates that manganese did not replace iron in the metal binding site of Y41F- or H155Q-*Ss*SOD. The analysis on the metal content allows a better expression of the specific activity of the different *Ss*SOD forms as U·mg protein^{-1}·mol of Fe^{-1}·mol subunit. The data reported in Table 3 indicate that the specific activity of *Ss*SOD is 17-fold reduced by the Y41F replacement, whereas it is only 1.7-fold reduced by the H155Q mutation.

Effect of Inhibitors and Inactivators on Y41F-SsSOD and H155Q-SsSOD. The activity of *Ss*SOD and its mutant forms was measured in the presence of increasing concentrations of sodium azide, a typical inhibitor of Fe- and Mn-SODs, that is otherwise ineffective on *Ss*SOD (*9*, *10*) also in its modified form (*13*). The dose-dependent inhibition profiles reported in Figure 2A indicate that Y41F-*Ss*SOD and, to a lesser extent, H155Q-*Ss*SOD are inhibited by sodium azide, whereas no inhibition at all occurs for the wild-type enzyme.

Hydrogen peroxide is an inactivator of Fe-SODs, acting on *Ss*SOD (*9*), also in its PMSF-modified form (*13*). The time course of the residual activity of wild-type and mutant *Ss*SOD forms treated with 0.5 mM hydrogen peroxide at 25

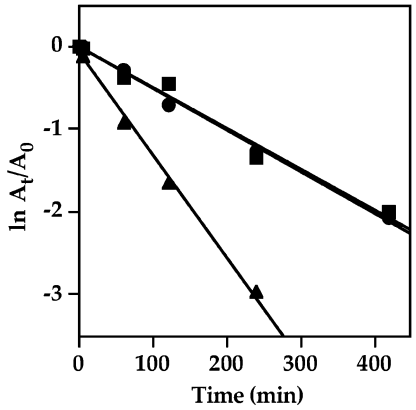

FIGURE 3: Heat inactivation at 99 °C of wild type and mutant forms of *Ss*SOD. Solutions of 0.1 mg/mL *Ss*SOD (●), Y41F-*Ss*SOD (■), and H155Q-*Ss*SOD (▲) in standard buffer were incubated at 99 °C. At the times indicated, aliquots were withdrawn from the incubation mixtures and assayed for residual SOD activity as described in Materials and Methods. Data were plotted according to a first-order kinetics.

°C is shown in Figure 2B. Compared to the inactivation kinetics of *Ss*SOD, that of Y41F-*Ss*SOD is slightly slower. On the other hand, a significantly faster rate of H_2O_2 inactivation is observed with H155Q-*Ss*SOD. This different sensitivity of the mutant forms of *Ss*SOD toward H_2O_2 was confirmed also in the presence of 0.1 mM hydrogen peroxide (not shown).

The effect of PMSF on mutant *Ss*SOD forms was determined by measuring their residual activities after a treatment with an increasing PMSF concentration (Figure 2C). While *Ss*SOD is progressively inactivated by this compound, no effect emerges for Y41F-*Ss*SOD or H155Q-*Ss*SOD up to 5 mM PMSF. The insensitivity of the mutant forms of *Ss*SOD is consistently observed even if the molar ratio inactivator/protein is varied in a large interval (not shown).

Effect of Heat and SDS on the Activity of SsSOD and Its Mutant/Modified Forms. It is known that *Ss*SOD is endowed with a very high heat resistance (*9*), which is even improved by the PMSF modification (*13*). In a first experimental approach to measure the effect of temperature on *Ss*SOD mutants, the heat stability of wild-type and mutant enzymes was evaluated by measuring their time-dependent residual activities after exposure at 99 °C (Figure 3). The data confirm the extreme thermoresistance of *Ss*SOD and indicate that Y41F-*Ss*SOD has a very similar inactivation kinetics. In contrast, a faster rate of heat inactivation is observed with H155Q-*Ss*SOD.

The inactivation of *Ss*SOD and its mutant and modified forms was also studied in the presence of the detergent SDS. In protein samples kept at 0 °C in the presence of 1% SDS, no significant time-dependent inactivation occurs for several hours. However, Y41F-*Ss*SOD showed a surprising improvement of its specific activity up to 1750 U·mg protein^{-1}·mol of Fe^{-1}·mol subunit. The combined effect of heat and detergent is shown in Figure 4, which reports the inactivation kinetics of wild-type and mutant/modified *Ss*SOD forms at 80 °C in the presence of 1% SDS. The data show that the detergent significantly decreases the stability of *Ss*SOD and accelerates its inactivation. A similar rate of inactivation is observed for H155Q-*Ss*SOD, whereas Y41F-*Ss*SOD and the PMSF-modified form of *Ss*SOD initially are inactivated with a similar rate but then more slowly, especially Y41F-*Ss*SOD.

Analysis of SsSOD and Its Mutant/Modified Forms by FT-IR Spectroscopy. The secondary structure and the thermal stability of wild-type and mutant/modified *Ss*SOD were analyzed by FT-IR spectroscopy. The deconvoluted infrared spectrum of *Ss*SOD recorded at 20 and 99.5 °C is shown in Figure 5A. The information on the protein secondary structure is contained in the 1700−1600 cm^{-1} interval, corresponding to the four bands forming the Amide I′ region (*39*). The spectrum obtained at high temperature shows only marginal differences in the Amide I′ region with respect to the spectrum recorded at 20 °C, indicating that *Ss*SOD is very resistant toward thermal denaturation. Similar results were obtained with the other mutant and modified forms of *Ss*SOD (spectra not shown). The FT-IR spectroscopy experiments were also carried out in the presence of SDS. The deconvoluted spectrum of *Ss*SOD at 20 °C in the absence and in the presence of SDS (Figure 5B) shows that the detergent has no effect on the protein secondary structure at 20 °C, because the Amide I′ bands are almost superimposable. In the presence of SDS, the Amide I′ region of Y41F-*Ss*SOD is very similar to that of *Ss*SOD (Figure 5C), thus indicating that this mutation does not alter the secondary structure of the enzyme at 20 °C. Similar results were obtained with H155Q-*Ss*SOD (Figure 5D) and PMSF-modified *Ss*SOD (Figure 5E).

The 1554.1 cm^{-1} band shown in Figure 5 is due to the residual Amide II band. In ^1H_2O medium the intensity of this band is about 2/3 of the Amide I band (not shown), but in ^2H_2O medium it decreases as a consequence of the exchange of amide hydrogen with deuterium (*40*). The larger the decrease in intensity, the larger the $^1H/^2H$ exchange, and in turn, the larger the accessibility of the solvent (^2H_2O) to the protein. Hence, the data of Figure 5 indicate that high temperatures, or SDS, or mutations allow a larger accessibility of the solvent to the protein. In turn, this effect could be attributable to a more flexible or less compact tertiary and/or quarternary structure (*41*), rather than to changes in the secondary structure. Thus, according to the residual Amide II band intensity, Y41F-*Ss*SOD (Figure 5C) and H155Q-*Ss*SOD (Figure 5D) would appear to be more flexible or less compact than *Ss*SOD, whereas PMSF-modified *Ss*SOD would show a flexibility/compactness almost similar to that of *Ss*SOD (Figure 5E). The last band marked in the *Ss*SOD spectrum (1514.1 cm^{-1}), assigned to tyrosine absorption (*42*), has been found slightly lower in intensity than the control (Figure 5C), as a consequence of the Y41F replacement.

The thermal denaturation patterns of wild-type and mutant/modified *Ss*SOD forms obtained through FT-IR measurements are shown in Figure 6. In the absence of SDS, the Amide I′ bandwidth of *Ss*SOD shows a small increase only at very high temperature, a feature preventing the observation of the thermal denaturation pattern (*43*). Similar results were obtained with the other proteins (not shown). On the other hand, in the presence of SDS, a significant increase of the Amide I′ bandwidth of *Ss*SOD is evident at high temperatures, even though the denaturation pattern of the wild-type enzyme is still incomplete. The H155Q replacement destabilizes the protein structure in the presence of SDS because the denaturation pattern of this mutant starts at a lower

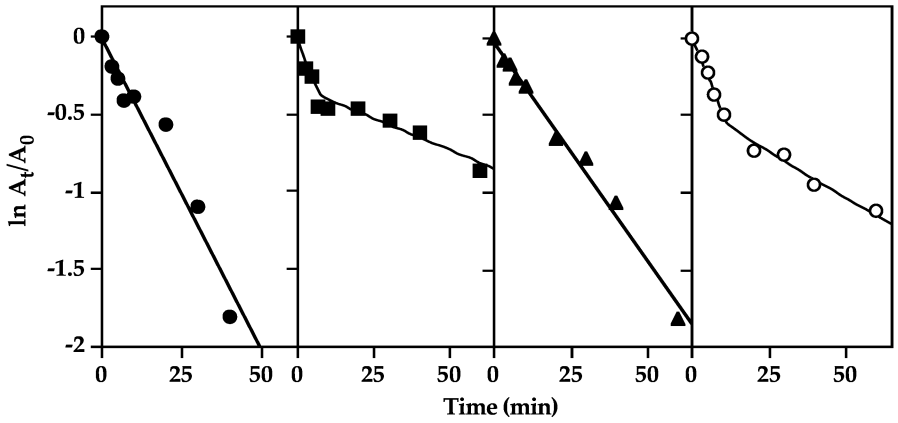

FIGURE 4: Heat inactivation at 80 °C of wild type, mutant, and modified forms of *Ss*SOD in the presence of SDS. Solutions of 0.1 mg/mL *Ss*SOD (●), Y41F-*Ss*SOD (■), H155Q-*Ss*SOD (▲), and a modified form of *Ss*SOD containing 55% of Y41 modification (○) in 50 mM Tris·HCl, pH 7.8, were incubated at 80 °C in the presence of 1% SDS. At the times indicated, aliquots were withdrawn from the incubation mixtures and assayed for residual SOD activity as described in Materials and Methods. Data were plotted according to a first-order kinetics.

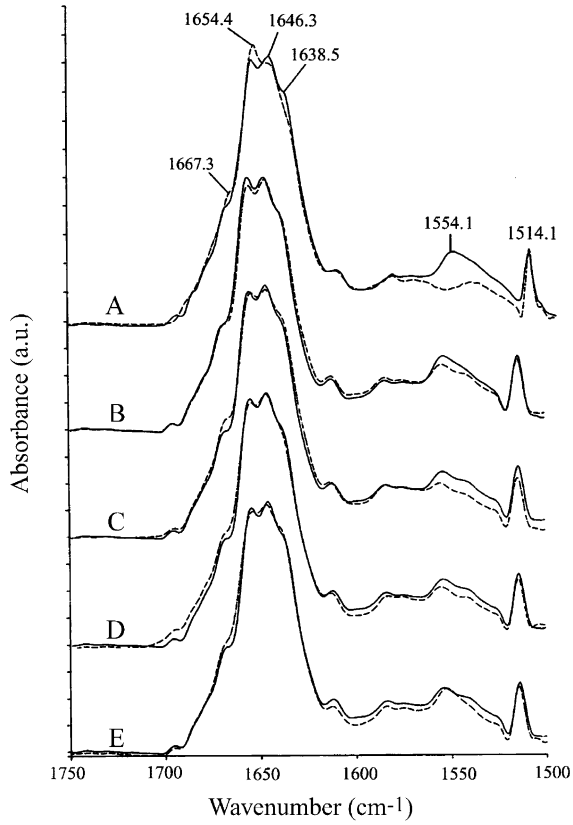

FIGURE 5: Effect of high temperature, SDS, Y41F, and H155Q mutations, and PMSF modification of Y41 on the deconvoluted FT-IR spectrum of *Ss*SOD. (A) Continuous and dashed lines refer to *Ss*SOD analyzed at 20 °C and 99.5 °C, p^2H 7.8, in the absence of SDS. (B) The proteins were analyzed at 20 °C, p^2H 7.8. Continuous and dashed lines refer to *Ss*SOD in the absence and in the presence of 5.6% SDS, respectively. (C−E) The proteins were analyzed in the presence of 5.6% SDS at 20 °C, p^2H 7.8. Continuous lines refer to *Ss*SOD. Dashed lines refer to Y41F-*Ss*SOD (C), H155Q-*Ss*SOD (D), and PMSF-modified *Ss*SOD (E).

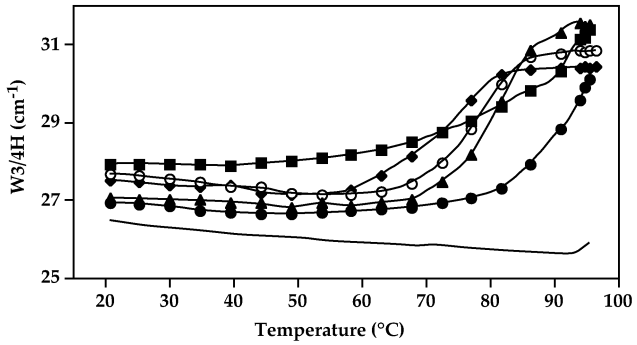

FIGURE 6: Thermal denaturation curves for *Ss*SOD, Y41F-*Ss*SOD, H155Q-*Ss*SOD, and PMSF-modified *Ss*SOD in the presence of 5.6% SDS. The curves were obtained by monitoring the Amide I′ bandwidth, calculated at 3/4 of Amide I′ band height (W3/4H), as a function of the temperature (*43*). All curves were obtained from protein samples in the presence of SDS, with the exception of the curve referred to a sample of *Ss*SOD in the absence of SDS (continuous line). Protein samples in the presence of SDS are: *Ss*SOD (●), Y41F-*Ss*SOD (■), H155Q-*Ss*SOD (▲), and a PMSF-modified *Ss*SOD containing 21% (○) or 70% (♦) modification.

temperature compared to *Ss*SOD and it is almost complete in the temperature range tested. Also, an increasing PMSF-modification of Y41 progressively destabilizes the structure of the enzyme in the presence of SDS. On the other hand, the denaturation pattern of Y41F-*Ss*SOD in the presence of SDS displays an unusual curve. First, the bandwidth increase starts at a lower temperature, indicating some protein structural changes. Second, the curve has a low gradient and increases significantly only at higher temperatures, when a marked denaturation occurs.

Y41F-SsSOD Crystal Structure. The Y41F mutant crystallized in the same space group as the PMSF-modified *Ss*SOD (*11*) and with similar cell constants (Table 1). The crystal packing is the same and the monomer structure is very similar to modified *Ss*SOD with an rms difference of 0.24 Å for the 205 ordered C_α atoms. There are no significant changes in the quaternary structure, including the interactions in the dimer interface of the conserved dimer. Besides the Y41F mutation itself, the only noticeable difference is in the surrounding solvent molecules. There is a solvent molecule 2.94 Å from the C_ζ atom of F41 (Figure 7) hydrogen bonding to $N_{\delta 1}$ of H155. This solvent molecule creates an uninterrupted hydrogen bond network from the iron-ligating hydroxide ion via H155 and two solvent molecules to H37. In *Ss*SOD this hydrogen bond network is most likely also present with the hydroxy group of Y41 replacing the solvent molecule interacting with H155. In the two SODs with both native and "Y41F" mutant structures available in the PDB, human mitochondrial Mn-SOD (refs *44* and *45*; PDB codes

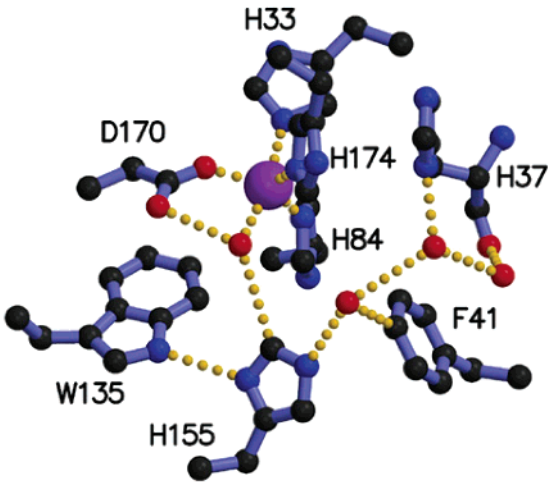

FIGURE 7: Active site of the Y41F mutant of *Ss*SOD. Some hydrogen bonds are represented by dotted yellow lines showing the hydrogen bond network connecting H37 via H155 to the iron-ligating hydroxide ion. Atom color: carbon, black; oxygen, red; nitrogen, blue; iron, purple. Water molecules are shown as red spheres. The figure was prepared with Molscript (*56*) and Raster3D (*57*).

1MSD and 1AP6), and *E. coli* Mn-SOD (refs *46* and *47*; PDB codes 1VEW and 1EN5), this hydrogen bond network is also present in the native structure, though in *E. coli* the distance from the second solvent molecule to $N_{\delta 1}$ of the residue corresponding to H37 is slightly long (3.5 Å) for an optimal interaction. However, in the Y34F mutants of these SODs, the hydrogen bond network is not present *(45*, *47)* because the mutant phenylalanine together with a tryptophan (in the position of *Ss*SOD F172) are sterically hindering a solvent molecule to enter to the position of the tyrosine hydroxy group (*47*).

DISCUSSION

Tyrosine 41 and histidine 155 are two interacting residues of the second coordination sphere in the active site metal center of *Ss*SOD. While Y41 is absolutely conserved, both the position and the identity of residue 155 (*Ss* numbering) undergo a conservative variation among Fe- and Mn-SODs. In Mn-SODs this residue belongs to the C-terminal domain of the enzyme, being often glutamine, or in a few cases histidine. In Fe-SODs a structurally equivalent residue occupies two alternative positions in the enzyme structure: indeed, it is a histidine or a glutamine in the C-terminal or N-terminal domain, respectively. Nonetheless, in all Fe- and Mn-SODs structures the conserved tyrosine is always hydrogen-bonded to the glutamine/histidine residue in the outer cordination sphere of the metal. Therefore, the comparison of our data on the mutagenesis of Y41 and H155 with the results of analogous mutations reported from other sources allows a better definition of the functional role of these residues.

Neither Y41F nor H155Q substitution affects the structural organization of *Ss*SOD in four identical subunits. From the metal analysis of wild-type and mutant proteins, a similar slight impairment of the iron content emerges after either Y41F or H155Q substitution. However, manganese does not replace the iron atom in the metal binding site of the mutant enzymes.

Concerning the importance of Y41 and H155 in the catalytic activity, several findings support the conclusion that the most relevant role in *Ss*SOD is played by the tyrosine residue. The deprotonation of the free hydroxy group of Y41 significantly impairs the catalysis of *Ss*SOD, as revealed from the large pH dependence of its activity. Also, the 17-fold decreased activity of Y41F-*Ss*SOD compared to wild-type enzyme, together with its pH independence, are in agreement with the crucial role played by Y41 during catalysis. This behavior is only partially similar to what is reported on the effects of tyrosine to phenylalanine mutations in other sources. Indeed, the calculated p*K* of 8.4 found for Y41 deprotonation is very similar to the corresponding value of 8.5 reported for Y34 ionization in Fe-SOD from *E. coli* (*17*), whereas in Mn-SODs a higher value was reported for either *Paracoccus denitrificans* (p*K* 9.8; ref *48*) or *E. coli* (p*K* 9.7; ref *49*). Furthermore, the Y34F replacement in Fe-SOD from *E. coli* (*17*, *18*) causes a reduction of activity to 40%, and in the Y34F mutant of human mitochondrial Mn-SOD the difference of activity between wild-type and mutant enzyme is even lower (*19*). However, in this latter case, the activity change becomes greater when a highly efficient catalysis is required by increased superoxide levels (*45*); the authors conclude that the absolute conservation of tyrosine through evolution could reflect constraints from extreme rather than average cellular conditions. Our data on the dramatic effect of the tyrosine to phenylalanine mutation in a hyperthermophilic source are in agreement with this hypothesis. A structural explanation for the higher activity reduction observed with the archaeal mutant enzyme could be the presence of the solvent molecule replacing the hydroxy group of Y41; in the corresponding mutant Mn-SOD from *E. coli* and human mitochondria the solvent molecule is absent. The extensive hydrogen bonding network created in the Y41F mutant could cause a tighter conformation of the active site, thus rendering the entrance of the substrate more difficult. A moderate treatment with SDS could possibly make the active site more accessible. In fact, under mild conditions this detergent specifically improves the activity of Y41F-*Ss*SOD; as a consequence, in these conditions the effect of the Y41F mutation on the activity becomes less dramatic compared to wild-type enzyme. On the other hand, the importance of the Y41 hydroxy group for catalysis has alreaby been proved by the PMSF treatment, which causes a steric hindrance to the active site (*13*).

The catalytic properties of H155Q-*Ss*SOD suggest that H155 is less directly involved in the mechanism of catalysis of *Ss*SOD. Indeed, this mutation produces less than a half-reduction of the activity and does not affect the p*K* of Y41 deprotonation. In Fe-SOD from *Mycobacterium tuberculosis*, the substitution of the wild-type histidine 146 (equivalent to H155 of *Ss*SOD) for glutamine or glutamate causes only small changes in the conformation of the surrounding residues (*24*). In the 3D-structures of *Ss*SOD (*11*) and *M. tuberculosis* Fe-SOD (*21*), the orientation of H155 or H146, respectively, is quite similar, the $C_{\epsilon 1}$ atom of histidine forming a hydrogen bond with the metal-bound hydroxyde ion. Furthermore, in the crystal structure of the H146Q mutant of *M. tuberculosis* Fe-SOD, a hydrogen bond is formed between Q146 and Y36, equivalent to Y34 of *Ss*SOD (Figure 8). Most likely, the H155Q replacement in *Ss*SOD still allows the formation of a weak hydrogen bond between

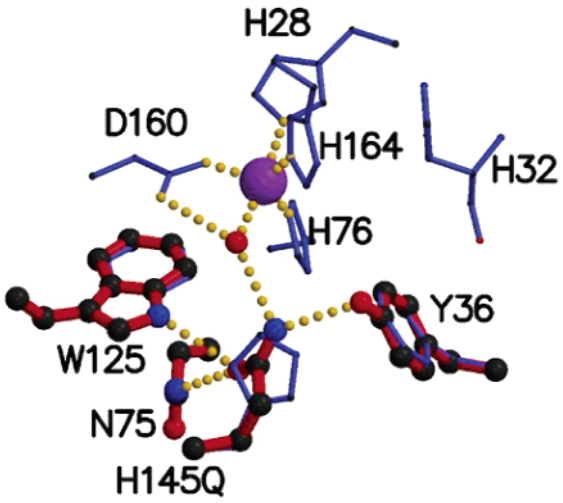

FIGURE 8: Active site of *M. tuberculosis* Mn-SOD H145Q mutant. The active site of *M. tuberculosis* wild-type structure (blue thin lines; ref *21*) with Y36, N75, W125, and Q145 of *M. tuberculosis* Mn-SOD H145Q mutant (*24*) shown in red. Some hydrogen bonds are shown as dotted yellow lines. The H145Q mutant corresponds to the H155Q mutant in *Ss*SOD. All of the shown residues are the same in *Ss*SOD except N75, which corresponds to *Ss*SOD L83, and thus there is no hydrogen bond between residue 155 and 83 in *Ss*SOD. Note that the *M. tuberculosis* Mn-SOD H145Q mutant model is determined at 4.0 Å resolution but the native model at 2.0 Å resolution. Atom color: carbon, black; oxygen, red; nitrogen, blue; iron, purple. Water molecules are shown as red spheres. The figure was prepared with Molscript (*56*) and Raster3D (*57*).

Y41 and Q155. The moderate reduction of activity found with H155Q replacement in *Ss*SOD is in agreement with this hypothesis. A somehow different picture emerges from the study of mutations on structurally equivalent positions in other sources. For instance, in *E. coli* Mn-SOD the replacement of the wild-type glutamine 146 for histidine (or other residues) has dramatic negative effects on the activity (*47*). Furthermore, the pH dependence of the activity is also somehow affected by some mutations. A similar picture emerges from the study of the Q143 mutants of human mitochondrial Mn-SOD (*50*, *51*). It is interesting to note that in the *E. coli* Mn-SOD the mutant histidine adopts a conformation sterically similar to that of the wild-type glutamine (*47*), which is different from that of the wild-type histidine in the iron-containing enzymes *Ss*SOD and *M. tuberculosis* SOD. The dramatic effects on the catalytic activity of glutamine to histidine mutations in Mn-SODs could be related to the different orientation of the histidine residue.

The sensitivity toward sodium azide acquired by Y41F- and H155Q-*Ss*SOD renders the archaeal enzyme more similar to other Fe- and Mn-SODs, even though its sensitivity remains significantly lower, even in the case of the most susceptible Y41F mutant. For instance, the inhibition observed in the presence of 30 mM sodium azide is only 42% and 15% for Y41F and H155Q mutants, respectively, whereas a 2 mM solution of this inhibitor is sufficient to cause a 50% inhibition of wild-type Fe-SOD from *E. coli*, and a 20-fold lower concentration is needed for the corresponding Y34F mutant (*18*). In the Y41F mutant the reduced steric hindrance could be responsible for its sensitivity toward sodium azide. The insensitivity displayed by the PMSF-modified *Ss*SOD (*13*) is in agreement with this hypothesis. Another possible explanation for the acquired sensitivity of both mutants resides in a less appropriate architecture of the active site region of *Ss*SOD caused by weaker bonding interactions as a consequence of the Y41F or H155Q replacement.

A previous study on the mechanism of hydrogen peroxide inactivation of Fe-SODs explains the sensitivity by a mechanism involving the oxidation of specific tryptophan residues, important for the enzymatic activity (*52*). In cambialistic SOD from *P. gingivalis* the target residue is W159 (*53*), whereas in *Propionibacterium shermanii* another position appears to be relevant because the substitution of valine 73 for a tryptophan residue turned the insensitive cambialistic SOD into a sensitive enzyme (*54*). However, in both cases the target tryptophan is close to the active site. A sequence alignment indicates that in *Ss*SOD no tryptophan residue is conserved in the above-mentioned positions (not shown). However, a candidate tryptophan could be W135, a residue quite close to the iron-binding position of *Ss*SOD (*11*). This hypothesis is reinforced by the occurrence of a hydrogen bond between W135 and H155, an interaction possibly weakened after H155Q replacement, and that would improve the accessibility of W135 to H_2O_2 inactivation.

The insensitivity to PMSF inactivation displayed by Y41F-*Ss*SOD mutant was expected since this mutant lacks the hydroxy group of tyrosine, target of the PMSF attack (*13*). In the other mutant, the lack of inactivation likely involves a missing modification of Y41. It is possible that in the H155Q mutant a weaker bonding interaction between Y41 and position 155 prevents the correct orientation of the hydroxy group of Y41 for the attack by PMSF, thus influencing the reactivity of Y41.

Concerning the structural role played by Y41 and H155 in maintaining the integrity of the active site of *Ss*SOD, the heat inactivation experiments carried out in the absence of SDS indicate that H155 contributes to the very high heat resistance of the enzyme, probably through the formation of two hydrogen bonds with Y41 and W135. In the H155Q mutant, these interactions are likely weakened, and this negatively disturbs the structural organization of the active site. Differently, the heat resistance of *Ss*SOD is fully retained in the Y41F mutant and even improved with the PMSF modification of Y41. The unique solvent molecule replacing the Y41 hydroxy group in the interactions between F41 with H155 probably contributes to the stability of Y41F-*Ss*SOD. The relevance of these amino acid positions in the heat stability of *Ss*SOD is apparently less evident upon the addition of SDS. However, an interesting observation comes from the surprising increased activity of Y41F-*Ss*SOD measured in the presence of SDS. A possible explanation for this effect is an enlargement of the active site channel caused by a better hydrophobic interaction between SDS and F41; in addition, a destruction of some relevant ion pairs in the intersubunit interactions cannot be excluded.

The FT-IR experiments indicate that the designed amino acid replacements or the covalent modification of Y41 does not affect the secondary structure of *Ss*SOD. On the other hand, in the presence of SDS the archaeal enzyme has a more flexible or less compact structure after either Y41F or H155Q substitution, but not after the covalent modification of Y41. The infrared spectra do not give direct information on protein sites where flexibility/compactness changes occur. In the

absence of changes or losses in secondary structure, an increase in $^1H/^2H$ exchange may be related to a relaxation of the whole tertiary/quaternary structure or of a particular part of the protein molecule, including the active site. A possible explanation of the FT-IR data is related to the fact that the Y41F replacement weakens the hydrogen bond interaction between F41 and H155, thus rendering this part of the molecule more flexible or less compact in the presence of SDS. A similar effect would occur with the H155Q replacement, but it would not occur with the covalent modification of Y41 because the oxygen of Y41, the acceptor of a hydrogen bond by H155, is retained after the covalent modification (*13*). The FT-IR data confirm the exceptional thermostability of *Ss*SOD because its denaturation pattern, although incomplete, is evident only upon the addition of SDS. Under these experimental conditions, the H155Q replacement and the presence of the Y41 modification cause a reduction of the thermostability of the enzyme, revealed as a general destabilization of the structure. However, the archaeal enzyme seems to retain in large part its great thermostability upon the Y41F replacement.

Some differences emerge from the comparison of our data with studies describing the effects of temperature on analogous mutations in other Fe- and Mn-SODs. Activity measurements proved that the Y34F mutant of Fe-SOD from *E. coli* has a decreased heat stability compared to wild-type (*18*). On the other hand, differential scanning calorimetry experiments showed that the Y34F mutant of human mitochondrial Mn-SOD has a transition temperature for thermal denaturation significantly higher than that reported for the wild-type enzyme (*45*). Similar studies of mutations in a position equivalent to H155 showed that the substitution of the wild-type glutamine 143 for histidine or asparagine in the human Mn-SOD does not essentially change the thermal denaturation temperature of this mitochondrial enzyme (*50*, *51*). However, nonconservative replacements of the same residue cause either an increase or a decrease of the unfolding transition temperature, depending on the ability of the mutated residues to re-form hydrogen bonds with the surrounding residues disrupted by the mutations (*51*). Another study on the effects of mutating a glutamine residue of Mn- or Fe-SOD from *E. coli* (Q146 or Q69, respectively) proved the involvement of this structurally conserved position (equivalent to H155 of *Ss*SOD) in the thermostability of the enzyme (*55*).

All these results point to different roles played by Y41 and H155 in *Ss*SOD. In particular, Y41 appears to be relevant for the catalytic properties of the enzyme, a free hydroxy group being strictly required for full activity of *Ss*SOD; if this group is deprotonated, blocked by PMSF, or abolished by mutation, the activity of the enzyme is greatly reduced. On the other hand, H155 is shown to be important for enzyme stability; it is likely that this residue plays an important role in keeping a correct structural architecture of the active site of *Ss*SOD. In other Fe- and Mn-SODs, a clear distinction among the functional roles of these residues is much less evident, both positions being involved in both catalysis and structural organization of the active site metal center of the enzyme. The study of the archaeal *Ss*SOD mutations opens new perspectives aimed at a better definition of the functional role of these residues.

ACKNOWLEDGMENT

We are indebted to lamented Prof. Vincenzo Bocchini for his initial encouragement and advice. We wish to thank Salam Al-Karadaghi for crystallographic data collection and Marco Trifuoggi for metal content analysis. We also thank Mariorosario Masullo and Andrea Parmeggiani for stimulating discussion and for critical reading of the manuscript.

REFERENCES

1. Keele, B. B., Jr., McCord, J. M., and Fridovich, I. (1970) Superoxide dismutase from *Escherichia coli* B. A new manganese-containing enzyme, *J. Biol. Chem. 245*, 6176−6181.
2. McCord, J. M., Boyle, J. A., Day, E. D., Jr, Rizzo, L. J., and Salin, M. L. (1977) A manganese-containing superoxide dismutase from human liver, in *Superoxide and Superoxide Dismutases* (Michelson, A. M., McCord, J. M., and Fridovich, I., Eds.) pp 129−138, Academic Press, London.
3. Fridovich, I. (1989) Superoxide dismutases. An adaptation to a paramagnetic gas, *J. Biol. Chem. 264*, 7761−7764.
4. Fridovich, I. (1986) Superoxide dismutases, *Methods Enzymol. 58*, 61−97.
5. Touati, D. (1988) Molecular genetics of superoxide dismutases, *Free Radical Biol. Med. 5*, 393−402.
6. Bannister, J. V., Bannister, W. H., and Rotilio, G. (1987) Aspects of the structure, function, and applications of superoxide dismutase, *CRC Crit. Rev. Biochem. 22*, 111−180.
7. Stallings, W. C., Metzger, A. L., Pattridge, K. A., Fee, J. A., and Ludvig, M. L. (1991) Structure−function relationships in iron and manganese superoxide dismutases, *Free Radical Res. Commun. 12*−*13*, 259−268.
8. Cannio, R., Fiorentino, G., Morana, A., Rossi, M., and Bartolucci, S. (2000) Oxygen: friend or foe? Archaeal superoxide dismutases in the protection of intra- and extracellular oxidative stress, *Frontiers in Biosci. 5*, 768−779.
9. Dello Russo, A., Rullo, R., Nitti, G., Masullo, M., and Bocchini, V. (1997) Iron superoxide dismutase from the archaeon *Sulfolobus solfataricus*: average hydrophobicity and amino acid weight are involved in the adaptation of proteins to extreme environments, *Biochim. Biophys. Acta 1343*, 23−30.
10. Yamano, S., and Maruyama, T. (1999) An azide-insensitive superoxide dismutase from a hyperthermophilic archaeon, *Sulfolobus solfataricus*, *J. Biochem. (Tokyo) 125*, 186−193.
11. Ursby, T., Adinolfi, B. S., Al-Karadaghi, S., De Vendittis, E., and Bocchini, V. (1999) Iron superoxide dismutase from the archaeon *Sulfolobus solfataricus*: analysis of structure and thermostability, *J. Mol. Biol. 286*, 189−205.
12. Lah, M. S., Dixon, M. M., Pattridge, K. A., Stallings, W. C., Fee, J. A., and Ludwig, M. L. (1995) Structure−function in *Escherichia coli* iron superoxide dismutase: comparison with the manganese enzyme from *Thermus thermophilus*, *Biochemistry 34*, 1646−1660.
13. De Vendittis, E., Ursby, T., Rullo, R., Gogliettino, M. A., Masullo, M., and Bocchini, V. (2001) Phenylmethanesulfonyl fluoride inactivates an archaeal superoxide dismutase by chemical modification of a specific tyrosine residue. Cloning, sequencing and expression of the gene coding for *Sulfolobus solfataricus* superoxide dismutase, *Eur. J. Biochem. 268*, 1794−1801.
14. MacMillan-Crow, L. A., Crow, J. P., Kerby, J. D., Beckman, J. S., and Thompson, J. A. (1996) Nitration and inactivation of manganese superoxide dismutase in chronic rejection of human renal allografts, *Proc. Natl. Acad. Sci. U.S.A. 93*, 11853−11858.
15. MacMillan-Crow, L. A., Crow, J. P., and Thompson, J. A. (1998) Peroxynitrite-mediated inactivation of manganese superoxide dismutase involves nitration and oxidation of critical tyrosine residues, *Biochemistry 37*, 1613−1622.
16. Yamakura, F., Taka, H., Fujimura, T., and Murayama, K. (1998) Inactivation of human manganese-superoxide dismutase by peroxynitrite is caused by exclusive nitration of tyrosine 34 to 3-nitrotyrosine, *J. Biol. Chem. 273*, 14085−14089.
17. Sorkin, D. L., Duong, D. K., and Miller, A. F. (1997) Mutation of tyrosine 34 to phenylalanine eliminates the active site p*K* of reduced iron-containing superoxide dismutase, *Biochemistry 36*, 8202−8208.
18. Hunter, T., Ikebukuro, K., Bannister, W. H., Bannister, J. V., and Hunter, G. J. (1997) The conserved residue tyrosine 34 is essential

for maximal activity of iron-superoxide dismutase from *Escherichia coli*, *Biochemistry 36*, 4925−4933.
19. MacMillan-Crow, L. A., and Thompson, J. A. (1999) Tyrosine modifications and inactivation of active site manganese superoxide dismutase mutant (Y34F) by peroxynitrite, *Arch. Biochem. Biophys. 366*, 82−88.
20. Miller, A. F., Padmakumar, K., Sorkin, D. L., Karapetian, A., and Vance, C. K. (2003) Proton-coupled electron transfer in Fe-superoxide dismutase and Mn-superoxide dismutase, *J. Inorg. Biochem. 93*, 71−83.
21. Cooper, J. B., McIntyre, K., Badasso, M. O., Wood, S. P., Zhang, Y., Garbe, T. R., and Young, D. (1995) X-ray structure analysis of the iron-dependent superoxide dismutase from *Mycobacterium tuberculosis* at 2.0 Ångstrom resolution reveals novel dimer-dimer interactions, *J. Mol. Biol. 246*, 531−544.
22. Borgstahl, G. E., Parge, H. E., Hickey, M. J., Beyer, W. F., Jr., Hallewell, R. A., and Tainer, J. A. (1992) The structure of human mitochondrial manganese superoxide dismutase reveals a novel tetrameric interface of two 4-helix bundles, *Cell 71*, 107−118.
23. Schmidt, M., Meier B., and Parak, F. (1996) X-ray structure of the cambialistic superoxide dismutase from *Propionibacterium shermanii* active with Fe or Mn, *J. Biol. Inorg. Chem. 1*, 532−541.
24. Bunting, K., Cooper, J. B., Badasso, M. O., Tickle, I. J., Newton, M., Wood, S. P., Zhang, Y., and Young, D. (1998) Engineering a change in metal-ion specificity of the iron-dependent superoxide dismutase from *Mycobacterium tuberculosis*. X-ray structure analysis of site-directed mutants, *Eur. J. Biochem. 251*, 795−803.
25. Yamakura, F., Sugio, S., Hiraoka, B. Y., Ohmori, D., and Yokota, T. (2003) Pronounced conversion of the metal-specific activity of superoxide dismutase from *Porphyromonas gingivalis* by the mutation of a single amino acid (Gly155Thr) located apart from the active site, *Biochemistry 42*, 10790−10799.
26. Borgstahl, G. E., Parge, H. E., Hickey, M. J., Johnson, M. J., Boissinot, M., Hallewell, R. A., Lepock, J. R., Cabelli, D. E., and Tainer, J. A. (1996) Human mitochondrial manganese superoxide dismutase polymorphic variant Ile58Thr reduces activity by destabilizing the tetrameric interface, *Biochemistry 35*, 4287−4297.
27. Karlin, S., and Campbell, A. M. (1994) Which bacterium is the ancestor of the animal mitochondrial genome? *Proc. Natl. Acad. Sci. U.S.A. 91*, 12842−12846.
28. Sambrook, J., Maniatis, T., and Fritsch, E. F. (1989) *Molecular Cloning. A Laboratory Manual*, Cold Spring Harbor Laboratory Press, Cold Spring Harbor, NY.
29. McCord, J. M., and Fridovich, I. (1969) Superoxide dismutase. An enzymic function for erithrocuprein (hemocuprein), *J. Biol. Chem. 244*, 6049−6055.
30. Bradford, M. (1976) A rapid and sensitive method for quantitation of microgram quantities of protein utilyzing the principle of protein-dye binding, *Anal. Biochem. 72*, 248−254.
31. Laemmli, U.K. (1970) Cleavage of structural proteins during the assembly of the head of bacteriophage T4, *Nature 227*, 680−685.
32. Salomaa, P., Schaleger, L. L., and Long, F. A. (1964) Solvent deuterium isotope effects on acid−base equilibria, *J. Am. Chem. Soc. 86*, 1−7.
33. D'Auria, S., Barone, R., Rossi, M., Nucci, R., Barone, G., Fessas, D., Bertoli, E., and Tanfani, F. (1997) Effects of temperature and SDS on the structure of β-glycosidase from the thermophilic archaeon *Sulfolobus solfataricus*, *Biochem. J. 323*, 833−840.
34. Cerenius, Y., Ståhl, K., Svensson, L. A., Ursby, T., Oskarsson, Å., Albertsson, J., and Liljas, A. (2000) The crystallography beamline I711 at MAX II, *J. Synchrotron Radiat. 7*, 203−208.
35. Kabsch, W. (1993) Automatic processing of rotation diffraction data from crystals of initially unknown symmetry and cell constants. *J. Appl. Crystallogr. 26*, 795−800.
36. Murshudov, G. N., Vagin, A. A., and Dodson E. J. (1997) Refinement of macromolecular structures by the maximum-likelihood method, *Acta Crystallogr. D53*, 240−255.
37. Brünger, A. T., Adams, P. D., Clore, G. M., DeLano, W. L., Gros, P., Grosse-Kunstleve, R. W., Jiang, J. S., Kuszewski, J., Nilges, M., Pannu, N. S., Read, R. J., Rice, L. M., Simonson, T., and Warren, G. L. (1998) Crystallography & NMR system: a new software suite for macromolecular structure determination, *Acta Crystallogr. D54*, 905−921.
38. Jones, T. A., Zou, J. Y., Cowan, S. W., and Kjeldgaard, M. (1991) Improved methods for building protein models in electron-density maps and the location of errors in these models, *Acta Crystallogr. A47*, 110−119.
39. Arrondo, J. L. R., Muga, A., Castresana, J., and Goñi, F. M. (1993) Quantitative studies of the structure of proteins in solutions by Fourier transform infrared spectroscopy, *Prog. Biophys. Mol. Biol. 59*, 23−56.
40. Osborne, H. B., and Nabedryk-Viala, E. (1982) Infrared measurements of peptide hydrogen exchange in rhodopsin, *Methods Enzymol. 88*, 676−680.
41. Barth, A., and Zscherp, C. (2002) What vibrations tell us about proteins, *Quarterly Rev. Biophys. 35*, 369−430.
42. Chirgadze, Y. N., Fedorow, O. W., and Trushina, N. P. (1975) Estimation of amino acid residue side-chain absorption in the infrared spectra of protein solutions in heavy water, *Biopolymers 14*, 679−694.
43. Scirè, A., Saccucci, F., Bertoli, E., Cambria, M. T., Principato, G., D'Auria, S., and Tanfani, F. (2002) Effect of acidic phospholipids on the structural properties of recombinant cytosolic human glyoxalase II, *Proteins 48*, 126−133.
44. Wagner, U. G., Pattridge, K. A., Ludwig, M. L., Stallings, W. C., Werber, M. M., Oefner, C., Frolow, F., and Sussman, J. L. (1993) Comparison of the crystal structures of genetically engineered human manganese superoxide dismutase and manganese superoxide dismutase from *Thermus thermophilus*: differences in dimer-dimer interaction, *Protein Sci. 2*, 814−825.
45. Guan, Y., Hickey, M. J., Borgstahl, G. E., Hallewell, R. A., Lepock, J. R., O'Connor, D., Hsieh, Y., Nick H. S., Silverman, D. N., and Tainer, J. A. (1998) Crystal structure of Y34F mutant human mitochondrial manganese superoxide dismutase and the functional role of tyrosine 34, *Biochemistry 37*, 4722−4730.
46. Edwards, R. A., Baker, H. M., Whittaker, M. M., Whittaker, J. W., Jameson, G. B., and Baker, E. N. (1998) Crystal structure of *Escherichia coli* manganese superoxide dismutase at 2.1-angstrom resolution, *J. Biol. Inorg. Chem. 3*, 161−171.
47. Edwards, R. A., Whittaker, M. M., Whittaker, J. W., Baker, E. N., and Jameson, G. B. (2001) Outer sphere mutations perturb metal reactivity in manganese superoxide dismutase, *Biochemistry 40*, 15−27.
48. Terech, A, Pucheault, J., and Ferradini, C. (1983) Saturation behavior of the manganese-containing superoxide dismutase from *Paracoccus denitrificans*, *Biochem. Biophys. Res. Commun. 113*, 114−120.
49. Whittaker, M. M., and Whittaker, J. W. (1997) Mutagenesis of a proton linkage pathway in *Escherichia coli* manganese superoxide dismutase, *Biochemistry 36*, 8923−8931.
50. Hsieh, Y., Guan, Y., Tu, C., Bratt, P. J., Angerhofer, A., Lepock, J. R., Hickey, M. J., Tainer, J. A., Nick, H. S., and Silverman, D. N. (1998) Probing the active site of human manganese superoxide dismutase: the role of glutamine 143, *Biochemistry 37*, 4731−4739.
51. Leveque, V. J. P., Stroupe, M. E., Lepock, J. R., Cabelli, D. E., Tainer, J. A., Nick, H. S., and Silverman, D. N. (2000) Multiple replacements of glutamine 143 in human manganese superoxide dismutase: effects on structure, stability, and catalysis, *Biochemistry 39*, 7131−7137.
52. Yamakura, F. (1984) Destruction of tryptophan residues by hydrogen peroxide in iron-superoxide dismutase, *Biochem. Biophys Res. Comm. 122*, 635−641.
53. Yamakura, F., Rardin, R. L., Petsko, G. A., Ringe, D., Hiraoka, B. Y., Nakayama, K., Fujimura, T., Taka, H., and Murayama, K. (1998) Inactivation and destruction of conserved Trp159 of Fe-superoxide dismutase from *Porphyromonas gingivalis* by hydrogen peroxide, *Eur. J. Biochem. 253*, 49−56.
54. Gabbianelli, R., Battistoni, A., Capo, C., Polticelli, F., Rotilio, G., Meier, B., and Desideri. A. (1997) Effect of Val73→Trp mutation on the reaction of "cambialistic" superoxide dismutase from *Propionibacterium shermanii* with hydrogen peroxide, *Arch. Biochem. Biophys. 345*, 156−159.
55. Hunter, T., Bannister, J. V. and Hunter, G. J. (2002) Thermostability of manganese- and iron-superoxide dismutases from *Escherichia coli* is determined by the characteristic position of a glutamine residue, *Eur. J. Biochem. 269*, 5137−5148.
56. Kraulis, P. J. (1991) MolScript: a program to produce both detailed and schematic plots of protein structures, *J. Appl. Crystallogr. 24*, 946−950.
57. Merrit, E. A., and Murphy, M. E. P. (1994) Raster3D version 2.0: a program for photorealistic molecular graphics, *Acta Crystallogr. D50*, 869−873.

BI035661Y